Stiffness from Disorder in Triangular-Lattice Ising Thin Films

Shi-Zeng Lin,[1] Yoshitomo Kamiya,[2,1] Gia-Wei Chern,[1] and Cristian D. Batista[1]
[1]Theoretical Division, T-4 and CNLS, Los Alamos National Laboratory, Los Alamos, New Mexico 87545, USA
[2]iTHES Research Group and Condensed Matter Theory Laboratory, RIKEN, Wako, Saitama 351-0198, Japan
(Received 11 October 2013; published 15 April 2014)

We study the triangular lattice Ising model with a finite number of vertically stacked layers and demonstrate a low temperature reentrance of two Berezinskii-Kosterlitz-Thouless transitions, which results in an extended disordered regime down to $T = 0$. Numerical results are complemented with the derivation of an effective low-temperature dimer theory. Contrary to order by disorder, we present a new scenario for fluctuation-induced ordering in frustrated spin systems. While short-range spin-spin correlations are enhanced by fluctuations, quasi-long-range ordering is precluded at low enough temperatures by proliferation of topological defects.

DOI: 10.1103/PhysRevLett.112.155702 PACS numbers: 64.60.F–, 05.50.+q

Introduction.—The antiferromagnetic triangular lattice Ising model (TLIM) is the paradigmatic example of geometric frustration [1–3]. Despite its simplicity, the TLIM exhibits all the defining features of a highly frustrated magnet. The extensive degeneracy of its ground state or Wannier manifold, which comprises any state without three parallel spins on the same triangle, leads to a residual entropy density $S \approx 0.323 k_B$. This property makes the system very sensitive to perturbations, as is manifested in the algebraic spin-spin correlations. Simple perturbations, such as further-neighbor couplings, relieve the frustration and induce long-range order (LRO) or quasi-LRO [4–8]. The ground state degeneracy can also be lifted via the order-by-disorder mechanism [9]. For instance, a vertical 3D stacking of TLIMs produces a low-T partially disordered antiferromagnetic (PDA) phase consisting of two ordered sublattices with opposite magnetizations and the third one that remains disordered [10–15]. By adding a transverse field, we obtain the quantum Ising model (QIM) that also contains a low-T PDA phase stabilized by quantum fluctuations [16–18].

In this Letter, we show an exotic classical spin liquid phase with unusual pseudocritical correlations in a simple generalization of the TLIM, namely, a vertically stacked finite number N_z of triangular layers. This new phase consists of a line of pseudocritical disordered states. Surprisingly, spins become more correlated at short distances with increasing temperature: the spin correlation falls off like $\sim r^{-\eta(T)} e^{-r/\xi}$ with the exponentially large correlation length, $\ln \xi \propto J/T$, and the short-distance effective power law decay becomes slower at higher T ($d\eta/dT < 0$) [19]. This is similar to Villain's order by disorder [9]. However, while thermal fluctuations increase short-distance spin-spin correlations, hence the stiffness of the effective field theory, quasi-LRO sets in only when the stiffness reaches a critical value necessary to suppress the proliferation of topological defects.

Our study is in part motivated by recent advances in film-growth techniques [20,21] and fabrication of artificial spin systems [22]. The model Hamiltonian is

$$\mathcal{H} = J \sum_{n=1}^{N_z} \sum_{\langle i,j \rangle} \sigma^z_{i,n} \sigma^z_{j,n} - J_z \sum_i \sum_{n=1}^{N_z} \sigma^z_{i,n} \sigma^z_{i,n+1}, \quad J > 0, \quad (1)$$

where $\sigma^z_{i,n} = \pm 1$ is an Ising spin at site i of the nth layer, and $\langle i, j \rangle$ runs over intralayer nearest-neighbor sites. We use open (periodic) boundary conditions along the vertical direction (in the ab plane). Although not essential, we assume a ferromagnetic (FM) interlayer exchange $J_z > 0$.

We will see that the phase diagram of $\mathcal{H}$ changes with N_z, but there is always an extended pseudocritical phase right above $T = 0$ [Fig. 2(b)]. The single-layer TLIM has no phase transition at any finite T. For $N_z > 1$, while thermal fluctuations also destroy the critical state at $T = 0$, the configurational entropy enhances the short-range in-plane correlations, leading to the classical spin liquid phase. For $N_z < N_{c1}$ the system remains disordered at any finite T and the peculiar low-T state crosses over to the high-T paramagnetic (PM) state. For $N_{c1} \leq N_z < N_{c2}$, fluctuations induce a Berezinskii-Kosterlitz-Thouless (BKT) transition to a critical phase that is destroyed by another BKT transition at a higher temperature of order J. Conversely, the lowest-T BKT transition defines a reentrant transition back to the disordered low-T regime. Finally, for $N_{c2} \leq N_z < \infty$, a PDA phase emerges in the middle of the BKT phase.

The degenerate ground states of the TLIM are related to dimer coverings [6,23] and fully packed loops [24] on the dual honeycomb lattice [25]. To account for the exotic low-T physics, we derive a low-energy dimer model. Entropic effects generate interdimer interactions and topological defects that control the low-T physics and quantitatively reproduce the results of our Monte Carlo (MC) simulations of $\mathcal{H}$. The global phase diagram is also obtained by a different mapping of $\mathcal{H}$ into a single-layer QIM.

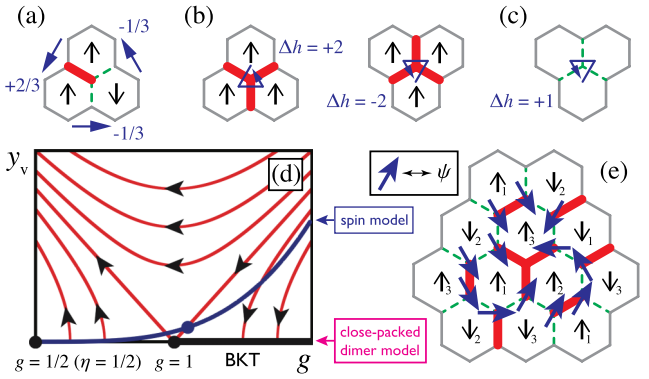

FIG. 1 (color online). (a) Mapping to a dimer state (each arrow stands for the majority spin of a chain). (b) Physical topological defects corresponding to height dislocations $\Delta h = \pm 2$. (c) Example of a monomer, which has no physical realization in the spin model. (d) Renormalization-group flow diagram near the lowest-T BKT transition ($g = 1$). The trajectory schematically shows the bare coupling of the spin model with $N_z > N_{c1}$, while the $y_v = 0$ axis corresponds to the close-packed dimer model. (e) Example of a vortex of the spin operator $\psi = \sigma_1^z + \sigma_2^z e^{2\pi i/3} + \sigma_3^z e^{4\pi i/3}$ associated with an isolated topological defect (note that three parallel spins correspond to $|\psi| = 0$, as expected for a vortex core).

Dimer coverings and effective low-T theory.—The highly degenerate ground space of $\mathcal{H}$ is also a Wannier manifold because it consists of FM vertical chains, which can be treated as effective Ising variables. This manifold is conveniently mapped onto the set of dimer coverings on the dual honeycomb lattice [6,23] by placing a dimer on every link that crosses a frustrated (i.e., up-up or down-down) bond [see Fig. 1(a)]. Because each triangle has only one frustrated bond, exactly one dimer is attached to each honeycomb lattice site. The $T = 0$ partition function of $\mathcal{H}$ is mapped onto a partition function for dimers with the same statistical weight for each dimer configuration.

By assuming $|J_z| < 2N_z J$, we can include thermal effects into an effective single-layer dimer model for $T \ll |J_z|$. We first consider lowest-energy excitations that create a single kink in a chain surrounded by three-up and three-down chains. The minimum excitation energy is $2|J_z|$, because the interchain molecular field is zero. Dressed by such kink excitations, these chains ($\hexagon$ or $\hexagon$ in the dimer representation) acquire a higher statistical weight $W \approx 1 + (N_z - 1)w$, where $w = \exp(-2|J_z|/T)$ and the prefactor $N_z - 1$ accounts for the possible locations of the kink along the chain. The finite-layer TLIM is then described by an action

$$\mathcal{S}_{\text{dimer}} = -K_3 \sum_i \left[n_i(\hexagon) + n_i(\hexagon) \right] + \cdots, \qquad (2)$$

where the dimer-covering constraint is implicit and $n_i(\cdot) = 1$ (0) if the plaquette i has (does not have) a designated dimer configuration and $K_3 = (N_z - 1)w + O(w^2)$. For simplicity, we have omitted the second-order terms (see the Supplemental Material [30]).

Because the low-T regime is close to the critical $T = 0$ state, we pursue an effective field theory to study the critical properties of the above dimer model. Following the standard approach [33–39], we assign a discrete height h_i to each plaquette i such that h_i changes by $2/3$ ($-1/3$) when crossing a dimer (empty link) while going counterclockwise around a site of one sublattice of the honeycomb lattice [Fig. 1(a)]. The dimer constraints assure a consistent height profile.

The critical spin states correspond to the roughing phase of the coarse-grained height field $h(\mathbf{r})$ described by a Gaussian theory. Taking into account the locking potential associated with the discreteness of the height variables, the effective long-wavelength theory is given by a standard sine-Gordon action,

$$\mathcal{S}_{\text{eff}} = \int d^2\mathbf{r}[\pi g(\nabla h)^2 + u_p \cos(2p\pi h)], \qquad p = 3. \qquad (3)$$

Here g is the stiffness and $u_{p=3}$ is the locking potential amplitude. In the Coulomb gas description equivalent to $\mathcal{S}_{\text{eff}}$ [40,41], the locking term carries an "electric" charge p and its scaling dimension is $\Delta_p = p^2/(2g)$. The locking potential becomes relevant for $g > 9/4$. Due to the periodicity in the height variable the dimer operator carries $p = 1$, i.e., $\Delta_{\text{dimer}} = 1/(2g)$, and we infer $g = 1/2$ for the TLIM at $T = 0$ [42] from the exact dimer correlator [43–45].

The fluctuation-induced dimer interaction increases the stiffness g because $K_3 > 0$ favors the columnar dimer state (flat landscape after coarse graining). In addition, an exponentially small but finite concentration of defects violating the constraint also appears at finite T. The simplest example is a triangle of parallel spin chains, which corresponds to a height dislocation $\Delta h = \pm 2$ [Fig. 1(b)]. These defects correspond to vortices of the spin operator ψ [46] with winding number ± 1 [Fig. 1(e)]. The factor of 2 arises because the associated vertex operator has $p = 1/2$, i.e., $\psi \sim \exp(i\pi h)$. Another crucial observation is that unitary ($\Delta h = \pm 1$) dislocations, namely monomers [see Fig. 1(c)], are *not* physical excitations of the spin model. Monomers are known to induce a three-state Potts transition [38]. The absence of monomers implies that our dimer model must undergo a BKT transition before reaching the ordered state.

After introducing height dislocations with $\Delta h = \pm 2$, the effective theory becomes a two-component Coulomb gas [40,41]. The dislocations $\Delta h = \pm 2$ carry a "magnetic" charge $q = \pm 2$ and have scaling dimension $\Delta_v = 2g$. Thus, although the bare defect fugacity y_v is exponentially small at low T, it is a relevant perturbation that destabilizes the critical $T = 0$ correlations: $\Delta_v \approx 1 < d = 2$ for $g \approx 1/2$. However, as the height field becomes stiffer with increasing

T, the defect fugacity y_v becomes irrelevant for $g > 1$, where the magnetic charges form bound pairs [Fig. 1(d)]. This is a massless BKT phase extending up to $g = 9/4$ where the locking term induces a flat (ordered) state. Our MC simulations (discussed below) show that this is the case for $N_z \geq N_{c1}$. Thus, our low-T theory predicts an extended pseudocritical regime right above $T = 0$ due to proliferation of unbounded defect triangles.

Quantum-classical mapping.—We can get a glimpse of the complete phase diagram of $\mathcal{H}$ by using the quantum-classical (QC) correspondence. We consider the single-layer QIM,

$$Z_Q = \mathrm{Tr}\,\exp\left(-\mathcal{H}_Q/T_Q\right),$$
$$\mathcal{H}_Q = J\sum_{\langle i,j\rangle}\sigma_i^z\sigma_j^z - \Gamma\sum_i \sigma_i^x, \tag{4}$$

where σ_i^μ are Pauli matrices at site i and we use a different symbol, T_Q, for the temperature of the QIM. The transverse field Γ selects the PDA ground state for $0 < \Gamma < \Gamma_c$ [17,18].

The order parameter space has a sixfold clock symmetry corresponding to the group generated by Z_3 lattice rotations and C_2 spin rotations around the x axis. Consequently, the finite-T_Q phase diagram is described by an effective six-state clock model [16–18]. For $0 < \Gamma < \Gamma_c$, the system undergoes two BKT transitions enclosing an intermediate critical phase with emergent U(1) symmetry [41] [see Fig. 2(a)].

By discretizing the imaginary time $[0, T_Q^{-1})$ into $N_\tau = N_z$ slices, the QIM is mapped to $\mathcal{H}$ with a periodic boundary condition in the vertical direction, whose effect becomes negligible in the large N_z limit. The mapping is given by $T = N_\tau T_Q$ and $J_z/T = -(1/2)\ln\tanh[\Gamma/(N_\tau T_Q)]$ (see the Supplemental Material [30] for details). While this mapping is exact only for $N_\tau \to \infty$, it is still a good approximation if $\Delta\tau \equiv T_Q^{-1}/N_\tau = T^{-1}$ is much smaller than the correlation length along the imaginary time axis ξ_τ. In this way we obtain

$$\Gamma(T, J_z) = T\tanh^{-1}\exp(-2J_z/T) \tag{5}$$

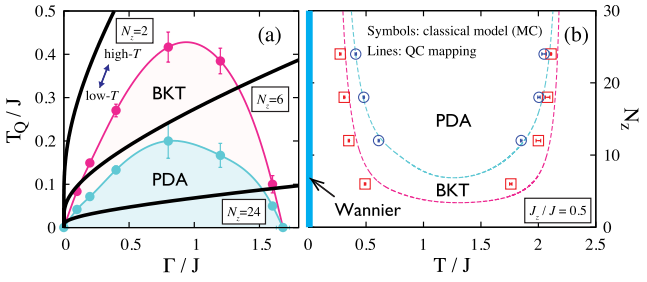

FIG. 2 (color online). (a) Phase diagram of the QIM (4) (data are MC results from Ref. [17]) and the trajectories of quasi-2D classical systems ($J_z/J = 0.5$; $N_z = 2$, 6, and 24). The phase boundaries are guides to the eye. (b) Phase diagram of the classical model compared with the QC mapping.

Thus, although $\mathcal{H}_Q$ per se does not exhibit "stiffness from disorder" (i.e., LRO sets in at low T_Q), varying T of the classical system corresponds to changing both T_Q and Γ in the phase diagram of the QIM. As is shown in Fig. 2(a), we expect three different scenarios depending on N_z and J_z/J in $\mathcal{H}$: (i) four BKT transitions with massless BKT and massive PDA phases, (ii) two BKT transitions with an intermediate massless phase, and (iii) a PM state at any $T > 0$. In particular, the disordered low-T regime predicted by the dimer model is confirmed by the QC mapping. Finally, because $\xi_\tau \simeq \Gamma^{-1}$ for $T_Q \ll J$, Eq. (5) implies that the QC mapping is only valid for $T \lesssim J_z$.

MC results of the spin model.—We confirm the above global phase diagram with direct MC simulations of $\mathcal{H}$ (see the Supplemental Material [30] for details). Below we fix $J_z/J = 0.5$ and change N_z to demonstrate the scenarios (i)–(iii). The order parameter of the PDA state is the $\mathbf{Q} = (2\pi/3, -2\pi/3, 0)$ Fourier component of the magnetization $\Psi = \sum_{s=1}^{3} M_s \exp[2(s-1)\pi i/3]$, where M_s is the sth sublattice magnetization ($1 \leq s \leq 3$) [17]. We also compute $C_6 = \langle \mathrm{Re}[\Psi^6]\rangle/\langle|\Psi|^6\rangle$ to distinguish LRO from quasi-LRO and the correlation function $G(\mathbf{r}) = \mathrm{Re}\langle\psi^*(\mathbf{r})\psi(0)\rangle$, where $\psi(\mathbf{r}) = N_z^{-1}\sum_n(\sigma^z_{\mathbf{r},n} + \sigma^z_{\mathbf{r}+\mathbf{e}_1,n}e^{2\pi i/3} + \sigma^z_{\mathbf{r}+\mathbf{e}_2,n}e^{4\pi i/3})e^{i\mathbf{Q}\cdot\mathbf{r}}$ is the local order parameter. C_6 equals -1 ($+1$) for perfect PDA (ferrimagnetic) order [17]. If the system has LRO, $R = G(L/2, 0)/G(L/4, 0)$ goes to unity for a lateral size $L \gg \xi$, while $R \to 0$ in the PM phase. R is particularly useful for detecting quasi-LRO because it becomes L independent when the system is critical [47].

The exponent η [see Fig. 3(a)] characterizing the spin-spin correlation function is estimated from the standard finite-size scaling hypothesis in $d = 2$ dimensions: $|\Psi| \sim L^{-\eta/2}$ (see Fig. S3 in the Supplemental Material [30]). This is a convenient quantity to locate BKT transitions because it takes a universal value. By analyzing scaling dimensions of perturbative operators that become marginal at each transition, Jose *et al.* have shown [41] that $\eta = 1/4$ ($\eta = 1/9$) at the BKT transition from the PM (PDA) state to the critical BKT phase. For instance, for the reentrant BKT transitions, we know that $\eta = 1/(4g)$ from the scaling dimension of ψ, while $g = 1$ and $g = 9/4$ for the lower and upper BKT transitions, respectively. η changes continuously between $1/4$ and $1/9$ in the critical phase.

Our simulation results for $N_z = 2$, 6, and 24 are summarized in Fig. 3, which clearly shows three distinct behaviors corresponding to the scenarios (i)–(iii). For $N_z = 24$, the ratio R becomes L independent in two temperature regimes in which the effective exponent η interpolates between $1/4$ and $1/9$, indicating two extended critical phases. A PDA phase, corresponding to a negative C_6, is sandwiched by these critical regimes. This LRO disappears in the $N_z = 6$ system (η never falls below $1/9$). Finally, for $N_z = 2$, the $R(T)$ curves for different L seem to merge at low temperatures. However, the corresponding

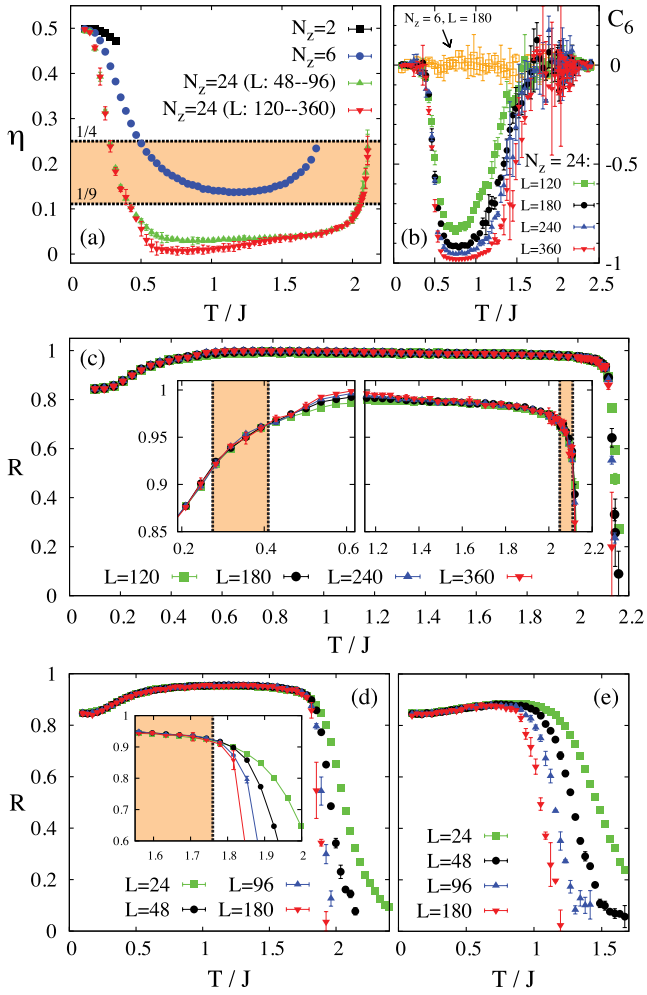

FIG. 3 (color online). (a) T dependence of the critical exponent η. (b) T dependence of C_6. (c)–(e) $R = G(L/2, 0)/G(L/4, 0)$ for $N_z = 24$, 6, and 2. The shaded regions in (a) and the insets of (c) and (d) indicate the BKT phase.

temperature range decreases systematically with increasing L, implying a PM state at any finite T [see Fig. 3(e)]. Interestingly, while $\eta_{\text{eff}} \gg 1/4$ confirms the PM nature at $T > 0$, the exponent approaches the $T = 0$ value ($\eta = 1/2$) from below. This is peculiar because the high-T trivial exponent is $\eta_{\text{eff}} = 2$ [48], and it indicates a crossover from an unstable fixed point [49]. The boundaries of the $(T/J, N_z)$ phase diagram shown in Fig. 2(b) agree quite well with the QC mapping. A small systematic shift is caused by the different boundary conditions in the vertical direction mentioned above.

The puzzling low-T physics can be explained with the aid of our low-energy dimer model. By using the directed-loop MC algorithm [50], we estimate the stiffness g by evaluating the winding number fluctuations [35,36] of the dimer model $\mathcal{S}_{\text{dimer}}$ (without defects) as a function of T, N_z, and J_z. The exponent $\eta = 1/(4g)$ must coincide with the effective exponent obtained from our MC simulations in the pseudocritical regime of the spin model ($\langle \sigma_{i,n}\sigma_{i+r,n}\rangle \sim r^{-\eta(T)}e^{-r/\xi}$)

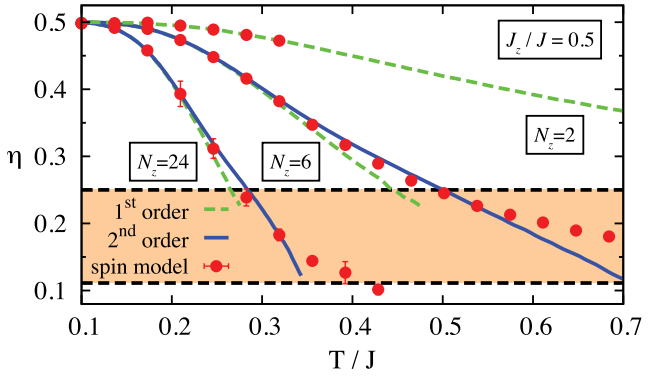

FIG. 4 (color online). Comparison of exponents in the low-T regime. The shaded region corresponds to the BKT phase (the horizontal lines indicate $\eta = 1/4$ and $\eta = 1/9$). The dashed (solid) lines are the results of simulating the dimer model with interactions up to first (second) order in w (error bars are smaller than the line width). The points are the results of MC simulations of the spin model [Fig. 3(a)].

because $\xi \propto y_v^{-1}$ is exponentially large in J/T and consequently much larger than L. For $N_z = 6$ and 24 we simulate both the first- [Eq. (2)] and second-order (see the Supplemental Material [30]) effective theories, while for $N_z = 2$ we use only the first order expression because second order contributions in w do not exist in this case. The excellent agreement between these results and those obtained directly from $\mathcal{H}$ (Fig. 4) confirms the validity of the effective low-T dimer model. The discrepancy at the lowest-T BKT transition (where $\eta = 1/4$) for $N_z = 6$ and 24 is $\lesssim 5\%$. Further discrepancies above the critical temperature indicate the breakdown of perturbation theory because K_3 [Eq. (2)] becomes of order 1.

In summary, the reentrant BKT transition of the TLIM with a finite number of vertically stacked layers leads to a low-T pseudocritical spin liquid phase. Based on a renormalization-group analysis of an effective dimer model, we unveiled the "stiffness from disorder" phenomenon that explains this exotic behavior. Our work underscores the subtle interplay between thermal fluctuations and topological defects. While thermal fluctuations enhance spin-spin correlations, quasi-LRO sets in only when the stiffness reaches the critical value required to suppress proliferation of topological defects. The ubiquitous nature of the Ising model offers alternative routes for realizing this exotic low-T physics. In particular, the multilayered TLIM described by $\mathcal{H}$ can be realized with thin films of $CsCoCl_3$ [4,51], buckled colloidal monolayers [52], or nanomagnet arrays [22].

We thank Y. Tomita, Y. Motome, A. Furusaki, H. Otsuka, H. Mori, and P. Chandra for valuable discussions. We also thank S. Isakov for providing his numerical data of the QIM. Computer resources for numerical calculations were supported by the Institutional Computing Program at LANL. This work was carried out under the auspices of

the NNSA of the U.S. DOE at LANL under Contract No. DE-AC52-06NA25396, and was supported by the U.S. DOE, Office of Basic Energy Sciences, Division of Materials Sciences and Engineering. Y. K. is grateful to the support by the RIKEN iTHES Project.

[1] G. H. Wannier, Phys. Rev. **79**, 357 (1950).
[2] R. Houtappel, Physica (Amsterdam) **16**, 425 (1950).
[3] K. Husimi and I. Syôzi, Prog. Theor. Phys. **5**, 177 (1950).
[4] M. Mekata, J. Phys. Soc. Jpn. **42**, 76 (1977).
[5] D. P. Landau, Phys. Rev. B **27**, 5604 (1983).
[6] B. Nienhuis, H. J. Hilhorst, and H. W. J. Blöte, J. Phys. A **17**, 3559 (1984).
[7] X. Qian and H. W. J. Blöte, Phys. Rev. E **70**, 036112 (2004).
[8] M. Sato, N. Watanabe, and N. Furukawa, J. Phys. Soc. Jpn. **82**, 073002 (2013).
[9] J. Villain, R. Bidaux, J. P. Carton, and R. Conte, J. Phys. (Paris) **41**, 1263 (1980).
[10] D. Blankschtein, M. Ma, A. N. Berker, G. S. Grest, and C. M. Soukoulis, Phys. Rev. B **29**, 5250 (1984).
[11] S. N. Coppersmith, Phys. Rev. B **32**, 1584 (1985).
[12] F. Matsubara and S. Inawashiro, J. Phys. Soc. Jpn. **56**, 2666 (1987).
[13] O. Heinonen and R. G. Petschek, Phys. Rev. B **40**, 9052 (1989).
[14] J.-J. Kim, Y. Yamada, and O. Nagai, Phys. Rev. B **41**, 4760 (1990).
[15] A. Bunker, B. D. Gaulin, and C. Kallin, Phys. Rev. B **48**, 15861 (1993).
[16] R. Moessner, S. L. Sondhi, and P. Chandra, Phys. Rev. Lett. **84**, 4457 (2000).
[17] S. V. Isakov and R. Moessner, Phys. Rev. B **68**, 104409 (2003).
[18] Y. Jiang and T. Emig, Phys. Rev. Lett. **94**, 110604 (2005).
[19] In contrast, the single-layer system ($N_z = 1$) does not exhibit such a peculiar enhancement of short-distance correlations.
[20] C. A. F. Vaz, J. A. C. Bland, and G. Lauhoff, Rep. Prog. Phys. **71**, 056501 (2008).
[21] D. P. Leusink, F. Coneri, M. Hoek, S. Turner, H. Idrissi, G. Van Tendeloo, and H. Hilgenkamp, arXiv:1309.2441.
[22] S. Zhang, J. Li, J. Bartell, X. Ke, C. Nisoli, P. E. Lammert, V. H. Crespi, and P. Schiffer, Phys. Rev. Lett. **107**, 117204 (2011).
[23] H. W. J. Blöte and H. J. Hilborst, J. Phys. A **15**, L631 (1982).
[24] H. W. J. Blöte and B. Nienhuis, Phys. Rev. Lett. **72**, 1372 (1994).
[25] Because the midpoints of the kagome lattice links form a honeycomb lattice, the TLIM is also relevant for systems such as kagome spin ice [26–28] and the kagome QIM [29].
[26] R. Moessner and S. L. Sondhi, Phys. Rev. B **68**, 064411 (2003).
[27] G. Möller and R. Moessner, Phys. Rev. B **80**, 140409 (2009).
[28] G.-W. Chern, P. Mellado, and O. Tchernyshyov, Phys. Rev. Lett. **106**, 207202 (2011).
[29] P. Nikolić and T. Senthil, Phys. Rev. B **71**, 024401 (2005).
[30] See Supplemental Material, which includes Refs. [31,32], at http://link.aps.org/supplemental/10.1103/PhysRevLett.112.155702 for details on the effective dimer model, the quantum-classical mapping, and numerical details and results.
[31] U. Wolff, Phys. Rev. Lett. **62**, 361 (1989).
[32] K. Hukushima and K. Nemoto, J. Phys. Soc. Jpn. **65**, 1604 (1996).
[33] J. Kondev and C. L. Henley, Phys. Rev. B **52**, 6628 (1995).
[34] J. Kondev and C. L. Henley, Nucl. Phys. **B464**, 540 (1996).
[35] F. Alet, J. L. Jacobsen, G. Misguich, V. Pasquier, F. Mila, and M. Troyer, Phys. Rev. Lett. **94**, 235702 (2005).
[36] F. Alet, Y. Ikhlef, J. L. Jacobsen, G. Misguich, and V. Pasquier, Phys. Rev. E **74**, 041124 (2006).
[37] S. Papanikolaou, E. Luijten, and E. Fradkin, Phys. Rev. B **76**, 134514 (2007).
[38] H. Otsuka, Phys. Rev. Lett. **106**, 227204 (2011).
[39] P. Chandra, P. Coleman, and L. B. Ioffe, Phys. Rev. B **49**, 12897 (1994).
[40] B. Nienhuis, J. Stat. Phys. **34**, 731 (1984).
[41] J. V. José, L. P. Kadanoff, S. Kirkpatrick, and D. R. Nelson, Phys. Rev. B **16**, 1217 (1977).
[42] This is consistent with the observation that $u_{p=3}$ is irrelevant with this stiffness.
[43] M. E. Fisher, Phys. Rev. **124**, 1664 (1961).
[44] H. N. V. Temperley and M. E. Fisher, Philos. Mag. **6**, 1061 (1961).
[45] P. W. Kasteleyn, J. Math. Phys. (N.Y.) **4**, 287 (1963).
[46] ψ can serve as an order parameter of both the PDA state and the up-up-down (or down-down-up) ferrimagnetic state.
[47] Y. Tomita and Y. Okabe, Phys. Rev. B **66**, 180401 (2002).
[48] M. Holtschneider, W. Selke, and R. Leidl, Phys. Rev. B **72**, 064443 (2005).
[49] Y. Kamiya, N. Kawashima, and C. D. Batista, Phys. Rev. B **82**, 054426 (2010).
[50] A. W. Sandvik and R. Moessner, Phys. Rev. B **73**, 144504 (2006).
[51] M. Mekata and K. Adachi, J. Phys. Soc. Jpn. **44**, 806 (1978).
[52] M. Harris, Y. Shokef, A. M. Alsayed, P. Yunker, T. C. Lubensky, and A. G. Yodh, Nature (London) **456**, 886 (2008).